Review of Hammershock Pressures in Aircraft Inlets

Louis C. Young* and Warren D. Beaulieu†
Rockwell International, Los Angeles, Calif.

Hammershock pressures caused by turbine engine stalls dictate the inlet duct structural design for high speed air vehicles. The initial pulse strength is defined by the inlet airflow cutoff rate, engine bypass ratio, and cycle pressure ratio. The inlet pressures are influenced by the inlet duct volume and area distribution and attenuation of the engine stall pulse by bypass or boundary-layer control air bleed from the duct. The scarcity of experimental data has inhibited in-depth hammershock analyses to date. The B-1 Inlet/Engine Compatibility Test model had very extensive dynamic pressure instrumentation. Deliberate engine stalls were made with off-design inlet geometry and/or by step engine fuel pulses. Data from the Arnold Engineering Development Center Propulsion Wind Tunnels test are utilized to show hammershock pressure propagation through the inlet duct. Test data will also be used to illustrate inlet design concepts for alleviation of transient pressure loads in the forward inlet region. The B-1 inlet-engine model test data enforce existing analytical and semi-empirical hammershock prediction techniques.

Nomenclature

A = area, ft^2, M^2
A_{th} = inlet throat area
A_2 = duct exit, engine inlet area
AIP = aerodynamic interface plane (fan front frame)
BLC = boundary-layer control (porous surface bleed in inlet)
CPR = compressor pressure ratio
ECS = environmental control system (specifically air scoop bleed from inlet)
FPR = fan pressure ratio
$FBPR$ = fan bypass pressure ratio (measured in fan bypass duct)
IDL = inlet distortion limit (inlet exit distortion pattern factor, an $IDL = 1$ denotes a pressure distortion pattern that will reduce the engine stall margin by 40 to 50%)
K = hammershock strength parameter ($K = 2.3$ for 100% flow cut-off)
LSW = lower sidewall (inlet wall remote from wing)
M = Mach number
M_2 = inlet exit/engine inlet Mach number
N = engine speed, rpm
P = pressure, psi, km^2
P_{HS} = hammershock pressure
P_2 = inlet exit static pressure
ΔP = pressure change (specifically, hammershock pressure increase)
P_{t3} = compressor discharge pressure
P_t = total pressure
P_{to} = freestream or wind tunnel total pressure
P_{t_2} = average total pressure at engine inlet
REC = pressure recovery, P_{t_2}/P_{to}
USW = upper sidewall (inlet wall adjacent to wing)
T = temperature, °Rankine
T_t = total temperature
W = weight flow lb/sec, k/sec
δ_t = total pressure/sea level standard pressure
Θ_t = total temperature/sea level standard temperature

Introduction

THE pressure pulse created by an engine stall/duct hammershock is the dominant inlet duct pressure load for tactical aircraft. The definition of inlet structural loads for future aircraft is hampered by the lack of experimental data to guide the analysis of a very complex problem. The engine stall pulse strength and duration is defined by the stall triggering mechanism, engine inlet Mach number, cycle pressure ratio, fan bypass ratio, and the fan-compressor interface geometry. The resulting pressure transients in the critical forward inlet region are dependent upon the strength of the pulse, the pre-stall flow conditions, the diffuser area distribution and volume, and attenuation by inlet bypass flow and the inlet boundary-layer control provisions.

This paper will discuss the effects of cycle variables on the strength of the hammershock pulse based upon published experimental data. Hammershock pressure transmission in the inlet duct will be illustrated by computer simulations and experimental data. Data from the recent B-1/F101 Inlet/Engine Compatibility Test in the Arnold Engineering Development Center Propulsion Wind Tunnel (PWT) will be presented. These PWT tests included 35 intentional engine stalls under controlled conditions with a variety of inlet geometry variables, engine stall initiation conditions, and with very extensive transient pressure instrumentation. The B-1/F101 test data will be utilized to illustrate turbofan engine transients during stall, the effects of pre-stall inlet flow conditions, and the duct pressure attenuation by inlet bypass bleed flow.

Background

Hard engine stalls were encountered during the F-107A aircraft flight test program. Post flight inspection after flight 52 showed that the throat ramp panels were buckled at the midpoint between the actuator link and the aft hinge as illustrated on Fig. 1. The photograph shows ramp

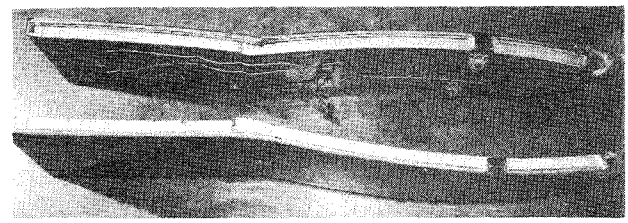

Fig. 1 F-107A hammershock damage. Buckled throat ramps discovered after flight 52, no F.O.D., no engine problems. Flight 74, $M_o = 2.04$, buzz induced rotating stall—110–115% $P_{T(o)}$ measured on duct wall at engine face.

Received September 11, 1974; revision received January 15, 1975.
Index categories: Aircraft Powerplant Design and Installation; Shock Waves and Detonations; Airbreathing Propulsion, Subsonic and Supersonic.

*Member of Technical Staff, Propulsion & Thermodynamics, Los Angeles Aircraft Division. Member AIAA.
†Member of Technical Staff, Propulsion System Aerodynamics, B-1 Division.

edge seal fractures, but there was no foreign object damage to the engine. Duct exit static pressures of 110–115% of freestream total pressure were measured during an inlet buzz induced rotating stall on a later flight. The hammershock pressures causing the inlet ramp failure were never measured.

The theoretical Mach number–hammershock pressure relationships for a sudden flow reduction are illustrated on Fig. 2. These P_{HS}/P_t vs Mach number curves were developed in Ref. 1 from the theory presented in Ref. 2. This paper will study the hammershocks originating with turbomachinery entrance Mach numbers of 0.3 to 0.5 and the resultant pressure pulses transmitted to the forward inlet region where the local Mach numbers range from subsonic to transonic.

Hammershock Source Pressure Trends

Turbofan engines soften, but also complicate the hammershock source strength and duration. Figure 3 illustrates a stall originating in the core compressor with a subsequent stall in the fan hub region. Alternatively, the stall can originate in the fan tip region or a sector of the fan and involve the compressor. The fan-compressor isolation gap noted on the figure has an important effect on both the stall sensitivity and pulse strength. A large gap will decrease the sensitivity of the compressor to fan distortion and bypass ratio transients. A large gap will also permit part of a compressor stall pulse to escape through the fan bypass duct and thereby reduce the back pressure of the fan and the resultant hammershock pressure in the inlet duct. The TF-30 engine has a tee fan-compressor geometry (fan and low pressure compressor stator on one rotor) and a very small isolation gap. TF-30 stall test data show that stalls consistently originated in the compressor and back-pressured the fan into stall. Although Fig. 2 relates the hammershock strength to the engine entrance Mach number, the volume dynamics of both the engine and inlet duct contribute to the hammershock pulse strength and duration.

Figure 4 presents a hammershock pressure correlation originated by Marshall. [3] Marshall's technique for collapsing the experimental data equates the hammershock pulse strength, $\Delta P/P_2$, to $K\,M_2^{1.26}$ where K is equal to 2.3 for a complete flow cutoff. The figure shows K increasing with cycle pressure ratio and decreasing with increasing fan bypass flow ratio. The shaded area enclosed NASA Lewis Research Center test cell data on TF-30 and GE1/10 engine stalls with 3 to 4 engine diameter length constant area ducts forward of the engine. As discussed in Ref. 4, the data scatter with a number of stall techniques obscure differences between stall pressure characteristics of the engine. The F101 engine, bypass ratio = 2+, shows low K levels for both fan and compressor initiated stalls in the

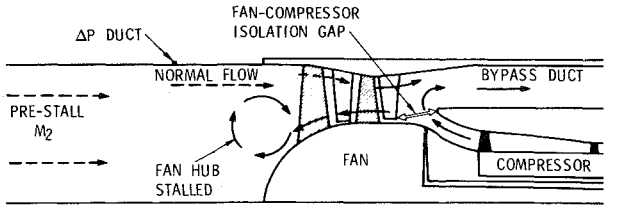

Fig. 3 Engine stall pressures. Note: majority of hard stalls originate in compressor; fan bypass duct offers path of least resistance—reduced duct Δp; fan-compressor isolation gap is critical to stall frequency and strength; increasing bypass ratio—less mass of stalled flow in compressor, more bypass duct volume for dump; H/S theory, $\Delta P \approx M_2$—but cycle pressure ratio indicates energy of stalled flow; stall pressure wave rarely uniform, poor instrumentation may not measure ΔP peak.

test cell. The inlet distortion induced stalls during the B-1 inlet/engine compatibility tests, flagged triangles, show very good agreement with the fan stalls in the previous GE full scale distortion tests of fan plus compressor test rig. These tests did not indicate significant $\Delta P/P_2$ differences between clean and distorted flow to the fan. The nominal bypass ratios are noted on the figure, the actual bypass ratio will increase with decreasing corrected engine speed, engine entrance Mach number, and cycle pressure ratio.

The designers of future tactical aircraft must be concerned about low to medium altitude, subsonic to low supersonic, penetration operations involving power transients and external flow disturbances conducive to engine stalls. The representative engine conditions will be: M_2, 0.4 to 0.5; cycle pressure ratio, 20; and K levels near 2. High altitude cruise at Mach numbers near 2 will involve M_2 near 0.3, cycle pressure ratio near 10, and above nominal bypass ratios that will reduce K levels to near unity. The $\Delta P/P_2$ levels at penetration will be 2 to 3 times the hammershock pressure ratios at supersonic cruise flight conditions.

Inlet Duct Pressure Trends

A thorough understanding of the transport of the hammershock pulse into the inlet duct requires a study of volume dynamics. An important tool for this research is the electronic computer simulation of airflow transients.

Figure 5 illustrates two hammershock simulations. The sketch on the left describes the Helmholz spring-mass resonator approach discussed in Refs. 5–9. An abrupt flow reduction is input to a small control volume at the engine entrance, station 2. The dynamic energy of the airflow entering the control volume is converted into an increase in

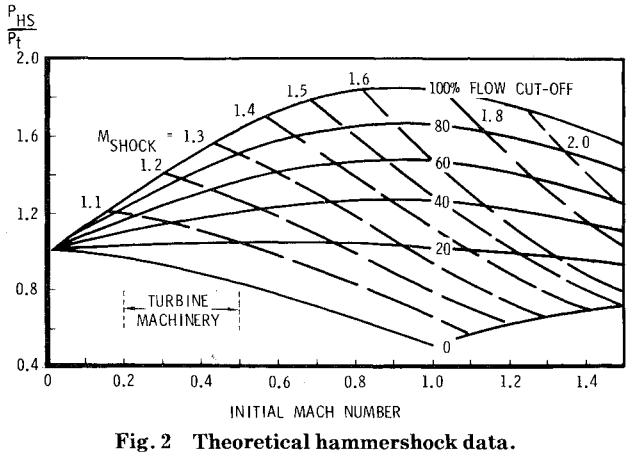

Fig. 2 Theoretical hammershock data.

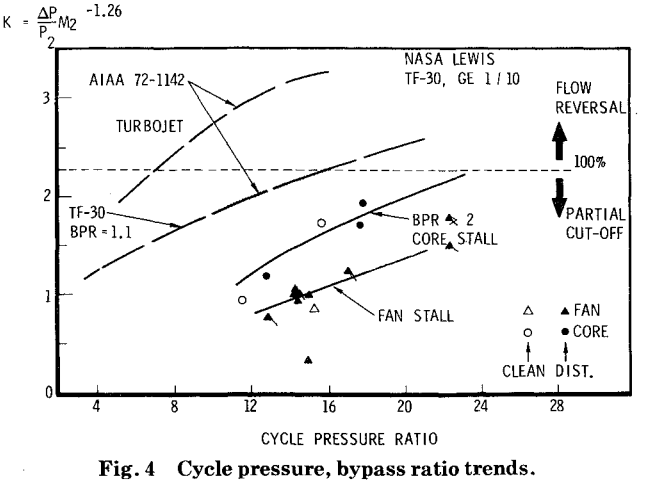

Fig. 4 Cycle pressure, bypass ratio trends.

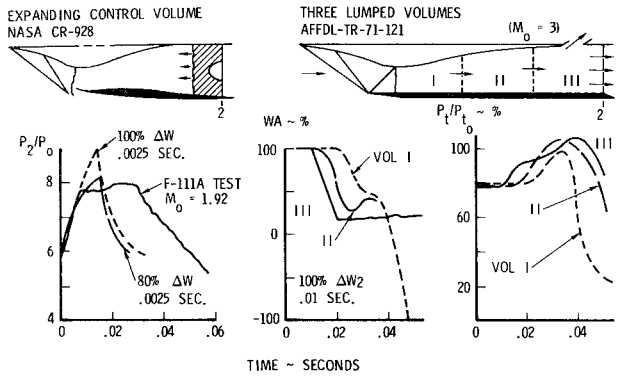

Fig. 5 Hammershock simulations.

static pressure in the control volume. As the disturbance front moves forward into the duct, the constant static pressure in the increasing control volume also increases until the disturbance front passes the cowl lip and diverts the freestream airflow. The left of the figure also presents a comparison of this simulation output to F-111A flight test hammershock pressures at the engine face.[10] A simulation input of an 80% flow reduction in 2.5 Msec showed good agreement with the flight pressure rise rate and maximum pressure, but the internal engine dynamics created a pressure plateau that this simulation could not duplicate.

The right side of Fig. 5 depicts the three lumped volume hammershock model of Ref. 11. This simulation utilizes a sequential balancing of the flow properties in each control volume. The example shows a Mach 3 flight case with about 20% of the inlet flow exiting through the bypass exit. A complete cutoff of the remaining 80% of the inlet flow in 10 Msec was input to volume III. The resulting inbalance of inflow and outflow in volume III created a static pressure rise which initiated a flow reduction in volume II about 3 Msec later. The flow continuity in volume I was upset in another 3 Msec. This simulation produced three distinct pressure peaks in the inlet duct and should improve the estimation of hammershock pressures in the forward inlet region.

Experimental inlet duct pressure distributions are compared on Fig. 6. The NASA Lewis model, left side, had four dynamic pressure transducers in one plane of the diffuser. It is significant that the transducers noted as 'C' and '2' were located in the channel formed by two of the three spike support struts. Also, the hammershock pressure peak at 'C' was greater than the engine stall pulse measured at point '2'. It appears that the bypass plenum, shown on the figure, with bypass exit closed, increased the effective volume of the channel and augmented the hammershock pressure at point 'C'. The hammershock pressure decreased rapidly as the wave passed points 'B' and 'A' and approached the inlet throat. If the initial stall pulse was essentially confined to one channel, the rapid increase in duct flow area near 'B' would spread the hammershock front and decrease the pressure. The effects of air bleed through the porous spike surface and the merging of the hammershock with the terminal normal shock contributed to the further hammershock pressure decay at point 'A'.

F-111A flight test hammershock pressure increments are shown on the right side of Fig. 6. The NASA Flight Research Center hammershock tests,[13] were completely independent from the Convair hammershock flight tests discussed in Ref. 14. The engine stalls were created by closing the inlet throat area to drive the inlet into a supercritical, high distortion condition; therefore, the prestall duct static pressures could not be accurately measured with the flight test data equipment used in this program. Estimations of prestall flow conditions and conversations with the authors of the NASA report indicated that the absolute hammershock pressure was probably about 150% $P_{t(o)}$ throughout the length of the inlet. The more extensive cowl pressure instrumentation of the tests discussed in Ref. 14 showed slightly higher pressures in the inlet throat as compared to the engine face hammershock pressures. The experimental data of Fig. 6 promise little forward duct pressure attenuation for a simple inlet and little help for predicting pressure loads in the throat region of complex inlets.

Inlet Duct Attenuation Techniques

Two processes that can relieve the pressures in the forward inlet duct are sketched in Fig. 7. The left side of the figure shows how airflow bleed through a bypass exit effectively reduces the volume of the diffuser. The result is a significant reduction in hammershock pressure, but experimental verification is not available from the published data. The right side of the figure sketches the use of leakage through the ramp edges and ramp boundary-layer bleed holes or slots. Inlet variable ramps normally have 0.5–1.0 in. edge gaps covered by spring steel seals. High pressure deflection of these seals can permit air leakage and pressure transmission at sonic velocity through the ramp boundary bleed plenum. The hammershock moves forward over the ramp surface at a relative Mach number of 0.7–0.8. If the ramp bleed plenum pressure rise precedes the hammershock pressure front by the time interval, Δt, shown on the figure, a worthwhile reduction in ramp pressure differential could be realized. The pressure differential across these edge seals will be about 1 to 2 lb/in.^{2} during sustained cruise operations, but can exceed 20 lb/in.^{2} during hammershocks encountered in high $P_{t(o)}$ penetration conditions. Significant

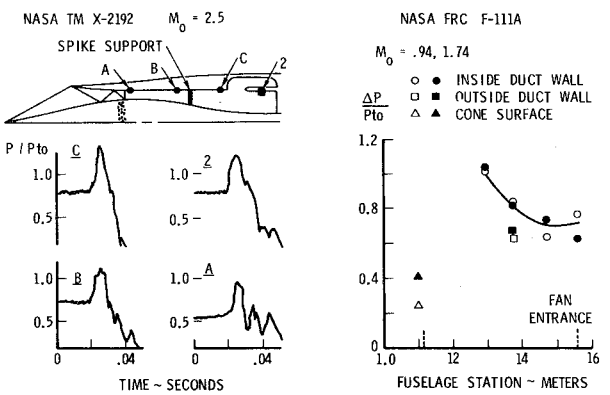

Fig. 6 Experimental hammershock pressures.

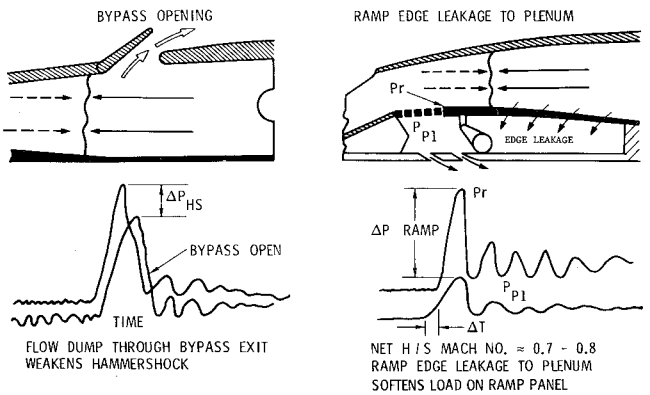

Fig. 7 Hammershock attenuation in duct.

weight reductions in inlet structure could be realized if the ramp or variable cone edge seals were designed to elastically unport under hammershock loads. Operation at limit pressure loads involve very short time spans and a very small percentage of the air vehicle life. For inlets incorporating a bypass system for supersonic operation, a small inlet bypass opening could be scheduled at high steady-state ram pressure conditions to provide a partial bleed of the hammershock pressure pulse. This technique will cause a performance loss for a very short time span. The concommitant reduction in design inlet load and structural weight may outweigh the increase in penetration mode fuel weight.

B-1/F101 Inlet/Engine Compatibility Test Program

The Arnold Engineering Development Center evaluation of the compatibility of the B-1 inlet and the F101 engine was conducted in the Propulsion Wind Tunnel (PWT) 16T tunnel in December 1973–January 1974 and the 16S tunnel in April 1974. The inlet was mounted in an inverted position to minimize flow interference from the support, Fig. 8, but the engine was mounted in a normal attitude. The model was maintained in a fixed attitude throughout the test. As illustrated in Fig. 9, the inlet model contained 35 high response pressure transducers in addition to the 40 total pressure transducers at the aerodynamic interface plane *(AIP)* at the fan front frame. The internal engine instrumentation included 26 high response pressure transducers. The pressure transducer data were recorded at 5000 Hz and digitized at 800 Hz for most of the data processing in this test.

The Rockwell/General Electric Interface Program developed the inlet distortion limit *(IDL)* as the combined steady-state and transient distortion patterns for the fan and compressor aerodynamic design. An *IDL* level of unity was estimated to use completely the fan stall line to operating line margin allotted to distortion. The remaining design pressure ratio margin was assigned to an engine acceleration margin, engine control tolerance, and service wear effects. During these tests, *IDL* levels well above unity were needed to create inlet distortion induced engine stalls.

The intentional engine stalls in the B-1 model tests included distortion stalls created by reducing the inlet throat area or opening the bypass door, engine accelerations with reduced throat area, supersonic buzz induced stalls by opening the inlet throat, and engine fuel pulse. The fuel pulse stall technique is described in the following paragraph.

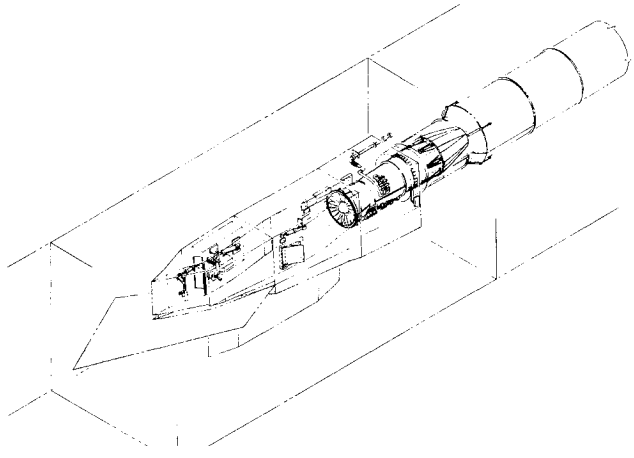

Fig. 8 B-1 full scale inlet/engine test AEDC. Inlet/engine-major details-*PWT*-16 ft transonic.

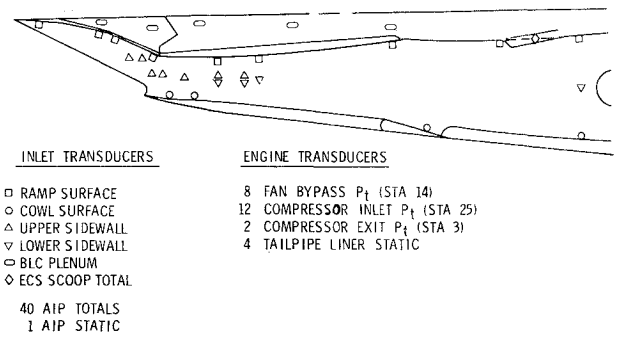

Fig. 9 Full scale test instrumentation.

Fuel Pulse Stalls

To create a fan stall a modification was made to the afterburner (A/B) fuel lines to allow the bypassing of the afterburner fuel recirculation to the facility when the engine was in A/B and then suddenly switching the fuel into the afterburner. A false $P_{s(3)}$ signal was applied to the A/B controller to cause a 50% increase in the amount of A/B fuel that was dumped into the afterburner. This step input in fuel resulted in the desired engine stalls.

A core stall was caused by an excessively rich fuel mixture in the main burner. The engine was controlled at part speed and a false $P_{s(3)}$ pressure was applied to the main fuel controller. This false $P_{s(3)}$ pressure affects only the acceleration fuel schedule. During the acceleration, the false $P_{s(3)}$ caused a 150% increase in fuel flow supplied to the main burner. This excessively rich fuel mixture caused a back pressure on the high-pressure compressor which resulted in a stall.

Inlet-Fan-Compressor Flow Interactions During Stall

Figure 10 presents the stall history for: a) a fuel pulse stall at subsonic conditions, b) an inlet distortion induced stall at subsonic conditions, and c) a supersonic distortion stall. The pressure ratios shown are: fan pressure ratio, *FPR* ($P_{t(25)}/P_{t(2)}$); fan bypass pressure ratio, *FBPR* ($P_{t(14)}/P_{t(2)}$); compressor pressure ratio, *CPR* ($P_{t(3)}/P_{t(25)}$); and the duct exit pressure recovery, $P_{t(2)}/P_{t(o)}$. The time slice of the fuel pulse stall shows a mild fan stall at the 50 Msec point which triggered a mild compressor stall at 55 Msec, this in turn created a hard fan stall at 61 Msec and a hard compressor stall about 8 Msec later. The average of the 40 total pressure transducers peaked at 136% $P_{t(o)}$ at the 71 Msec point. The hard compressor stall maintained a high-pressure plateau in front of the fan until about 85 Msec. For the distortion stall shown at (b), the engine was operated at intermedi-

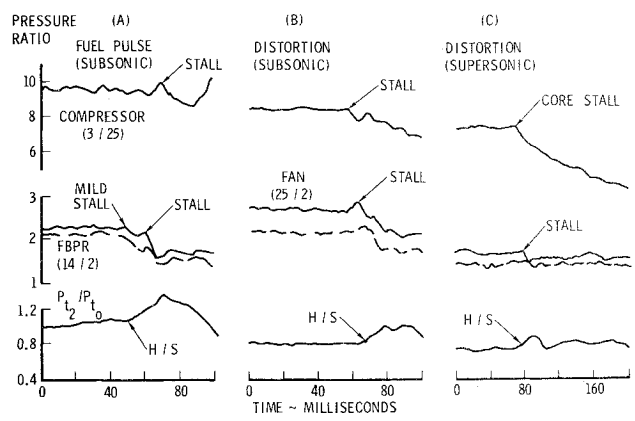

Fig. 10 Fan-compressor interactions during stall.

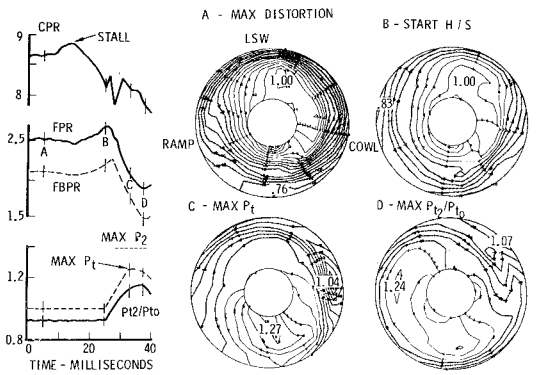

Fig. 11 Subsonic stall—distortion plus acceleration.

ate power while the throat area was reduced to about 53% of fan inlet area. The fan inlet distortion reached an *IDL* level of 1.4. The decay in fan hub performance, FPR, at 45 Msec initiated a compressor stall at 55 Msec and a following hard fan stall at 63 Msec. The drop in fan bypass duct pressure, *FBPR*, occurred about 2 Msec later. The inlet duct hammershock coincided with the *FBPR* stall. The fan inlet total pressure recovery showed a 16 Msec plateau with a peak hammershock delta pressure of about 20% $P_{t(o)}$.

The supersonic distortion stall, Fig. 10c, was created by opening the inlet bypass door. The inlet pressure recovery oscillated at 25 Hz and the inlet distortion limit, *IDL*, peaked at 1.31 just before the compressor stalled at 70 Msec in this time slice. The fan stalled at 78 Msec and the mild hammershock, ΔP = 12% $P_{t(o)}$, emerged as the inlet pressure recovery was on an increasing cycle.

The subsonic test stall on Fig. 11 was created by a combination of high inlet distortion, engine acceleration, and a main burner overtemperature induced by a false $P_{s(3)}$ signal to the fuel control. The inlet throat area was reduced to 59% of the fan inlet area with the engine controlled at part speed by the airflow limit signal (an inlet/engine control tie-in designed to limit engine air demand during supercritical inlet operation). When the airflow limit signal was switched out, the engine started accelerating and the false $P_{s(3)}$ signal created a main burner fuel pulse to displace the operating line. The compressor stalled as the fan speed reached 98% rpm. The right side of the figure presents selected fan inlet pressure profiles digitized at 800 Hz. The maximum and minimum total pressure points are noted on the profiles and the shaded regions denote sub-average total pressures. The inlet distortion peak at A caused a decay in fan pressure ratio which in turn created a hard compressor stall 8 Msec later. About 12 Msec later the fan stalled at B and a hard hammershock was initiated. The hammershock pressure plateau originated in the high pressure recovery region on the cowl side of the inlet and rotated around toward the ramp side with a ¾ revolution to the peak individual total pressure transducer reading of 127% $P_{t(o)}$ at C, 13 Msec later. The hammershock pressure plateau then spread into the ramp side region to the peak average fan inlet total pressure point, *D*. The fan pressure ratio started to recover at point D, but the compressor stall continued to the end of the data record. This very hard stall sequence required a combination of causes and; therefore, this event cannot be considered as representative of a service type stall and hammershock. However, these data provide insight to inlet-engine interactions during the stall-hammershock phase.

Typical Inlet Duct Hammershock Pressure Distributions

Figures 12–15 present static pressures, $P/P_{t(o)}$, vs station in the B-1 inlet duct. The open symbols denote prestall pressures. The solid symbols show the peak hammershock pressures measured at 5000 Hz. The half-solid symbols illustrate pressures averaged over a 3 Msec time period. During the XB-70 flight test program the strain gages mounted on inlet duct frames lagged the duct wall pressure transducers by about 2 Msec during inlet pressure transients. It appears that the structural elasticity of the inlet may absorb the very brief pressure peaks. The representative inlet design pressure loads should be between the solid and half-solid pressure symbols.

Figure 12 shows duct static pressures for the subsonic distortion induced stall illustrated on Fig. 10b. The static pressure transducer data on the inside cowl wall are noted by circle symbols, the ramp surface pressures are denoted by squares, and the pressures on the upper sidewall *(USW)* and lower sidewall *(LSW)* are denoted by triangular symbols. The elliptical symbols locate the ramp boundary-layer bleed plenum pressures *(BLC)* and a diamond symbol shows the total pressure in the environmental control system *(ECS)* scoop for ram cooling air for the engine bleed air precooler. It should be noted that the duct exit static pressures averaged 128% $P_{t(o)}$ with a peak of 142% $P_{t(o)}$ vs a 99% average and 118% $P_{t(o)}$ peak pressure for the fan inlet total pressures. It appears that the fan inlet total pressure probes were subject to the "reversed total pressure tube" error in measuring a suction pressure below the local static pressure due to reverse flow past the pitot tube. The hammershock pressure ratios for the average of the three duct exit static pressures show good agreement with the 100% flow cutoff curve of Fig. 2. It appears that the highest pressures behind the fan discharged directly into the low distortion, high total pressure, region at the duct exit.

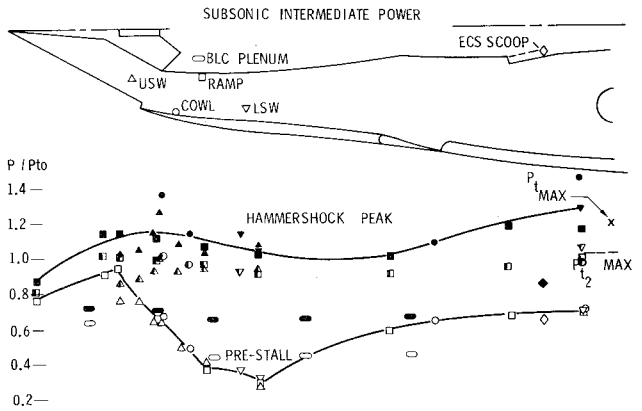

Fig. 12 Throat closure distortion stall.

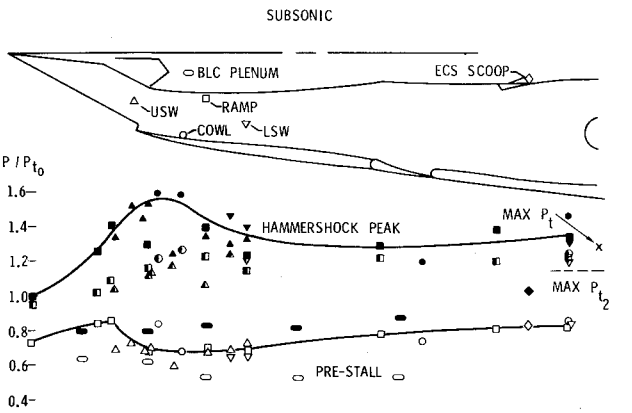

Fig. 13 Duct pressures—distortion and acceleration stall.

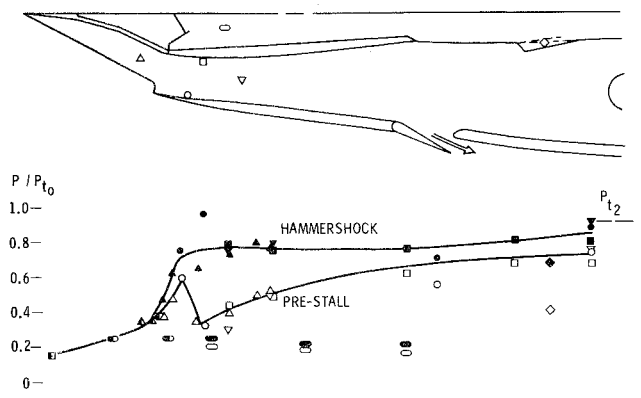

Fig. 14 Supersonic distortion stall duct pressure.

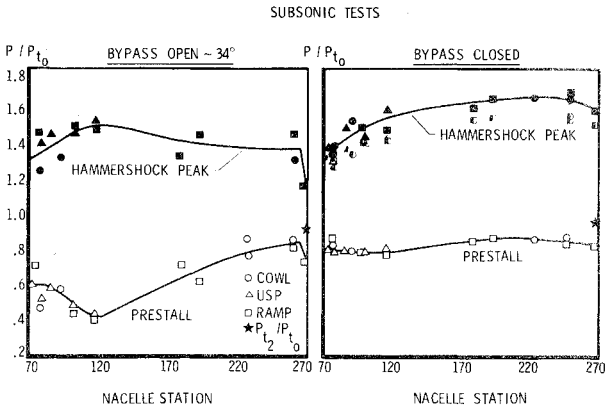

Fig. 15 Effect of bypass position on hammershock loads.

The average hammershock pressures decayed about 10% between the duct exit and inlet throat region. The prestall flow conditions approached Mach 1.4 in the supercritical region behind the inlet throat. The *BLC* II exits from the throat ramp bleed air plenum are closed at subsonic flight on the B-1 inlet, and the ramp edges were closed by inflated bulb seals; therefore, the beneficial effects of bleed plenum pressurization postulated in Fig. 7 could not be demonstrated during testing with this inlet.

The duct static pressures of Fig. 13 were measured from the subsonic distortion plus acceleration stall shown on Fig. 11. The average of the three duct exit static pressures is 137% $P_{t(o)}$ max and 122% $P_{t(o)}$ for 3 Msec as compared to the total pressures shown in Fig. 11. The 5000 Hz data in the inlet throat region show very high pressure peaks, but the 3 Msec average static pressures in the forward inlet are comparable to the duct exit 3 Msec average data.

Figure 14 depicts the prestall and peak hammershock pressures for a bypass transient induced distortion stall at supersonic speed. The mild hammershock at the engine face was predictable from the source pulse trends of Fig. 4. The absolute hammershock pressure level decayed in the forward region of the duct. Also, the hammershock delta pressures were insignificant forward of the cowl lip. The inherent increase in engine bypass ratio with ram temperature contributed to the mild hammershocks during supersonic testing with this propulsion system.

Effect of Inlet Bypass

Figure 15 compares the duct pressures for fuel pulse induced engine stalls with the bypass closed and with the bypass door opened to the 34° position. The bypass corrected airflow was about ⅓ of the engine corrected airflow; as a result, the inlet was forced into a supercritical mode with local Mach numbers near 1.2 behind the throat. This bypass opening decreased the prestall inlet total pressure recovery by 3.5% and the duct exit peak hammershock pressure by 30% of tunnel total pressure. The hammershock pressures in the inlet throat region, nacelle station 70 to 100, were only decreased by 5 to 6% of tunnel total pressure. It appears that a smaller bypass opening, with all subsonic inlet flow, would have shown more significant results. These data could provide validation for a simulation study of bypass flow effects on hammershock distribution.

Fuel pulse stalls with several bypass positions were made during the supersonic tests. A preliminary study of these data proved inconclusive. The fuel pulse back pressure always forced the inlet to an unstable condition before the hammershock in the 16S tests. The prestall duct pressures were located between the buzz cycle peak and bucket, the relatively small hammershock delta pressures were lost in the buzz amplitude pressures.

Conclusions

The hammershock pressure loads on the inlet duct are dominant design factors for tactical aircraft. The problem is particularly critical if variable geometry in the throat region is employed due to the complex load paths and basically inefficient structure necessary for rectangular inlets. An overly conservative design will result in excessive weight and a degraded mission performance. An optimistic design can result in loss of the aircraft either totally or for an extensive period of repair.

There is a growing body of engine test cell data to facilitate defining the effects of fan bypass ratio, engine cycle pressure ratio, and internal engine geometry on the strength of the source pressure pulse for a variety of stall initiation methods. These data should be further clarified to separate the exploratory stall test data from the predictable results due to service-type stall-triggering effects. The next step should be the modification of the refined test cell data to account for the area distribution and volume of aircraft inlet ducts. Computer simulations are necessarily one-dimensional in nature and must be validated with experimental data on the more complex flow processes that occur in service aircraft.

The differential hammershock pressure load on inlet variable geometry components may be reduced by selective pressurization of inlet boundary bleed air plenums or by anticipatory opening of the bypass exit to reduce the effective volume of the inlet duct. The second technique has been illustrated with data from the recent B-1/F101 inlet/engine compatibility test in the Arnold Engineering Development Center.

Conceptual design studies are being initiated on interdiction type air vehicles for operation in high ram air pressure environments. The volume and weight of the inlet ducts will have an impact on the weight, cost, and mission effectiveness of these aircraft. The inlet type and location effects on mission fuel consumption should be traded against inlet weight. The mission fuel costs of hammershock load alleviation techniques such as bypass exit opening during penetration operations should be balanced against structural weight reductions.

The aircraft and engine designers should undertake cooperative efforts to explore design techniques for minimizing the frequency and strength of engine stalls and hammershocks in high ram pressure operation. Moderate compromises in engine weight, volume, and cycle efficiency would be justified by overall propulsion system weight reductions and improved weapon system performance and survivability.

References

[1]Sedgewick, T. A., Brown, A. C., and Stroud, J. F., "Correlation of Wind Tunnel and Flight Test Data on the Air Induction

System of the F-104 Aircraft," WADC TR-1756, 1959, Wright Air Development Center, Wright-Patterson Air Force Base, Ohio.

[2]Rudinger, G., *Wave Diagrams for Non-Steady Flow In Ducts,* Van Nostrand, New York, 1955.

[3]Marshall, F. L., "Prediction of Inlet Overpressures Resulting From Engine Surge," *Journal of Aircraft,* Vol. 10, May 1974, pp. 274–278.

[4]Kurkov, A. P., Soeder, R. H., and Moss, J. E., "Investigation of the Stall-Induced Shock Wave (Hammershock) at the Inlet to the Engine," TMX-71594, Sept. 1974, NASA.

[5]Martin, A. W., "Propulsion System Dynamic Simulation Theory and Equations," CR-928, April 1967, NASA.

[6]Martin, A. W., and Wong, H. W., "Propulsion System Dynamic Simulation Users Manual," CR-73113, April 1967, NASA.

[7]Martin, A. W., and Kostin, L. C., "Propulsion System Dynamic Test Results," CR-73114, April 1967, NASA.

[8]Martin, A. W., "Propulsion System Dynamic Simulation Data," CR-73115, April 1967, NASA.

[9]Martin, A. W. and Beaulieu, W. D., "XB-70 Flight Test Data Comparison With Simulation Predictions of Inlet Unstart and Buzz," CR-1631, June 1969, NASA.

[10]Johnson, R. H., "B-1 Hammershock Estimates," NA 70-38, Aug. 1970, Rockwell International, Los Angeles, Calif.

[11]Amin, N. F. and Hall, G. R., "Supersonic Inlet Investigation, Air Induction System Dynamic Simulation Model," AFFDL-TR-121, Vol II, Sept. 1971, Air Force Flight Dynamics Lab., Wright-Patterson Air Force Base, Ohio.

[12]Choby, D. A., Burstadt, P. L., and Calogeras, J. E., "Unstart and Stall Interactions Between a Turbojet Engine and an Axisymmetric Inlet With 60-Percent Internal-Area Contraction," TMX-2192, March 1971, NASA.

[13]Nugent, J. and Holtzman, J., "Flight-Measured Inlet Pressure Transients Accompanying Engine Compressor Surges on the F-111A Airplane," TND-7696, June 1974, NASA.

[14]Barnard, J. D. and Evans, P. J., "Air Induction System Engine Stall Loads," *Proceedings of Third Structural Loads Workshop for Preliminary Aerospace Design Projects,* Aeronautical Systems Division, Wright-Patterson Air Force Base, Sept., 1970, pp. 89–127.

[15]Randall, L. M., et al., Rockwell Propulsion System Aerodynamics, "B-1 Full Scale Inlet-Engine Compatibility Test, AEDC TF 329 and SF 166, Vol. I, Preliminary Summary," NA-74-375, Aug. 1974, Arnold Engineering Development Center, Tullahoma, Tenn.

APRIL 1975 J. AIRCRAFT VOL. 12, NO. 4

Distortion-Induced Vibration in Fan and Compressor Blading

C. E. Danforth
General Electric Company, Cincinnati, Ohio

In contrast with the widespread tendency to rate the acceptability of inlet distortion patterns for airbreathing engine systems in terms of indices only stall related, this paper seeks to underline the importance of rating distortion characteristics specifically in their potential for inducing blade fatigue. In survey perspective, 8 mechanisms of distortion-induced vibration are described, only one of which has previously been discussed in the literature. While precision in each mechanism still represents a challenge to further research in steady and nonsteady aerodynamics, it is proposed that distortion characteristics can be identified specifically relevant to assessing blade resonance, random vibration in separated flow, and flutter, including a tentative approach to response in nonsteady distortion. A distortion index for blade vibration is defined both as an initial vibration design alert and for automatically assuring integration of design for inlet aerodynamics with that for blading.

I. Introduction

ONE wonders if highly important advances made in recent years by government and industrial research in the understanding and control of distortion-induced compressor stall margin degradation, may not have induced a preoccupation with this area with the result of slighting of another end product of a viable engines—life, as implied in freedom from distortion-induced blade vibratory fatigue. Underlying technologies of stall and blade vibration are indeed interdependent; even early formulations of nonsteady aerodynamics, initially developed for wing flutter, have contributed to stall understanding.[1-3] Blade aspect ratio trends benefitting stall margin usually help minimize vibration design challenges. Blade vibration signatures have contributed to performance gains and stall diagnosis. But extra severity distortion investigations tailored to stall margin demonstrations can also create blade vibration problems unrelated to actual service.

Preoccupied with performance aspects of distortion, are we not tempted to define designs and their applications relative to distortions acceptable in terms of indices that are only stall related? Usually performance degradation is given as a function of increasing distortion index in a low-to-moderate range. Structural damage is precluded up to

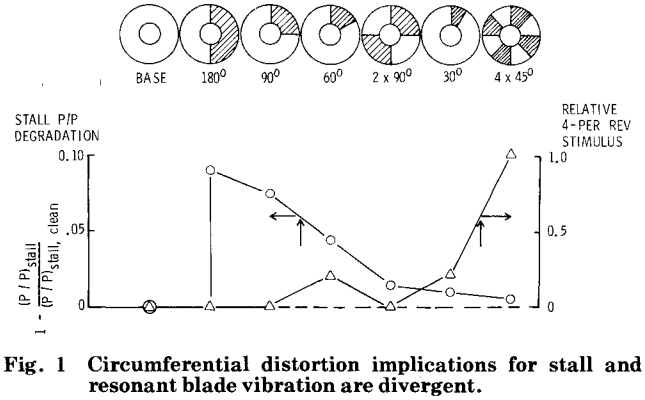

Fig. 1 Circumferential distortion implications for stall and resonant blade vibration are divergent.

Presented as Paper 74-232 at the AIAA 12th Aerospace Sciences Meeting, Washington, D.C., January 30–February 1, 1974; submitted October 29, 1974; revision received March 17, 1975. The author gratefully acknowledges the opportunity of writing this paper and permission granted by the General Electric Company to publish it.

Index categories: Airbreathing Propulsion, Subsonic and Supersonic; Structural Dynamic Analysis; Aircraft Powerplant Design and Installation.

*Chief Consulting Engineer, Aeromechanics, Aircraft Engine Group. Associate Fellow AIAA.